Long-term in vivo degradation behavior and near-implant distribution of resorbed elements for magnesium alloys WZ21 and ZX50

Journal Article

Author(s):
Amerstorfer, Florian; Fischerauer, Stefan F.; Fischer, Lisa; Eichler, Jens; Draxler, Johannes; Zitek, Andreas; Meischel, Martin; Martinelli, Elisabeth; Kraus, Tanja; Hann, Stephan; Stanzl-Tschegg, Stefanie E.; Uggowitzer, Peter; Löffler, Jörg F.; Weinberg, Annelie Martina; Prohaska, Thomas S.

Publication date:
2016-09-15

Permanent link:
https://doi.org/10.3929/ethz-b-000119894

Originally published in:
Acta Biomaterialia 42, https://doi.org/10.1016/j.actbio.2016.06.025

Acta Biomaterialia 42 (2016) 440–450

Contents lists available at ScienceDirect

Acta Biomaterialia

journal homepage: www.elsevier.com/locate/actabiomat

Full length article

Long-term *in vivo* degradation behavior and near-implant distribution of resorbed elements for magnesium alloys WZ21 and ZX50

F. Amerstorfer [a], S.F. Fischerauer [b], L. Fischer [c], J. Eichler [a], J. Draxler [d], A. Zitek [d], M. Meischel [e], E. Martinelli [a], T. Kraus [f], S. Hann [c], S.E. Stanzl-Tschegg [e], P.J. Uggowitzer [g], J.F. Löffler [g], A.M. Weinberg [a,*], T. Prohaska [d]

[a] Department of Orthopedic and Orthopedic Surgery, Medical University of Graz, 8036 Graz, Austria
[b] Department of Trauma Surgery, Medical University of Graz, 8036 Graz, Austria
[c] University of Natural Resources and Life Sciences, Department of Chemistry, Division of Analytical Chemistry – IACM Laboratory, 1190 Vienna, Austria
[d] University of Natural Resources and Life Sciences, Department of Chemistry, Division of Analytical Chemistry – VIRIS Laboratory, 3430 Tulln, Austria
[e] Department of Material Sciences and Process Engineering, Institute of Physics and Materials Science, University of Natural Resources and Life Sciences, 1190 Vienna, Austria
[f] Department of Pediatric Orthopedics, Medical University of Graz, 8036 Graz, Austria
[g] Laboratory of Metal Physics and Technology, Department of Materials, ETH Zurich, 8093 Zurich, Switzerland

ARTICLE INFO

Article history:
Received 5 May 2016
Accepted 17 June 2016
Available online 22 June 2016

Keywords:
Magnesium
Alloy
Yttrium
Long-term
Degradation
Distribution

ABSTRACT

We report on the long-term effects of degrading magnesium implants on bone tissue in a growing rat skeleton using continuous *in vivo* micro-Computed Tomography, histological staining and Laser Ablation Inductively Coupled Plasma Mass Spectrometry (LA-ICP-MS). Two different magnesium alloys—one rapidly degrading (ZX50) and one slowly degrading (WZ21)—were used to evaluate the bone response and distribution of released Mg and Y ions in the femur of male Sprague-Dawley rats. Regardless of whether the alloy degrades rapidly or slowly, we found that bone recovers restitutio ad integrum after complete degradation of the magnesium implant. The degradation of the Mg alloys generates a significant increase in Mg concentration in the cortical bone near the remaining implant parts, but the Mg accumulation disappears after the implant degrades completely. The degradation of the Y-containing alloy WZ21 leads to Y enrichment in adjacent bone tissues and in newly formed bone inside the medullary space. Locally high Y concentrations suggest migration not only of Y ions but also of Y-containing intermetallic particles. However, after the full degradation of the implant the Y-enrichment disappears almost completely. Hydrogen gas formation and ion release during implant degradation did not harm bone regeneration in our samples.

Statement of Significance

Magnesium is generally considered to be one of the most attractive base materials for biodegradable implants, and many magnesium alloys have been optimized to adjust implant degradation. Delayed degradation, however, generates prolonged presence in the organism with the risk of foreign body reactions. While most studies so far have only ranged from several weeks up to 12 months, the present study provides data for complete implant degradation and bone regeneration until 24 months, for two magnesium alloys (ZX50, WZ21) with different degradation characteristics. μCT monitoring, histological staining and LA-ICP-MS illustrate the distribution of the elements in the neighboring bony tissues during implant degradation, and reveal in particular high concentrations of the rare-earth element Yttrium.

1. Introduction

Magnesium has long been considered as one of the most attractive biodegradable materials, because it occurs as a natural (trace) element in the human body [1]. It is involved in many metabolic reactions and biological mechanisms [2] and can be easily excreted through the urinary tract [3,4]. When implanted as a medical device, magnesium reveals adequate biological response [3,5] and demonstrates excellent properties for fracture stabilization, as its elastic modulus occurs to be similar to that of human bone [6]. Magnesium also shows stimulatory effects on the growth of

* Corresponding author at: Department of Orthopedics and Orthopedic Surgery, Medical University Graz, Auenbruggerplatz 5, 8036 Graz, Austria.
E-mail address: anneliemartina.weinberg@medunigraz.at (A.M. Weinberg).

http://dx.doi.org/10.1016/j.actbio.2016.06.025
1742-7061/

adjacent new bone tissues [7–11]. Indeed the most outstanding feature of Mg-implants is, however, their ability to completely degrade in a living organism, which would render an additional surgery for implant removal in many clinical cases unnecessary [5,6,12–14]. However, the corrosion process of magnesium in physiological environment (pH at 7.4–7.6, high ion content, presence of proteins) is fairly rapid and is accompanied by the formation of hydrogen gas, which can cause tissue irritation and reduce mechanical integrity [6,10,13,15,16]. The degradation performance of a magnesium implant should therefore be balanced with the bone's healing process to provide sufficient primary fracture stabilization and prevent malunion or refracture at later stages. Hence, mechanical implant integrity over a time scale of at least 3 months in adults [17,18] and 1.5 months in children is essential.

For this purpose, various magnesium alloys have been tailored with the aim of optimizing degradation behavior by using appropriate alloying elements, surface modifications, coatings, or various processing techniques [14,19–28]. However, delayed degradation behavior involves prolonged implant presence in the organism and an attendant risk of foreign body reactions. Because most available studies cover observation periods from a few weeks to only 12 months, information on long-term effects until full implant degradation and beyond are still lacking. Additionally, rare-earth elements (REEs) such as Yttrium (Y) have been used in many Mg alloy designs to increase the strength, ductility, and corrosion resistance of the metal [29,30]. The issue that arises with REEs, however, is a lack of knowledge regarding their body clearance and potential effects on the physiological system. A recent comparative study by Rössig et al. in fact reported that REEs accumulate in inner organs after implant degradation [31]. Further research into the systemic and local long-term effects of REEs is needed to enable precise statements about their suitability for clinical implementation.

We have already reported on the *in vivo* degradation and biological response of REE-free versus Y-containing alloys (ZX50 and WZ21) over a period of 9 months [5]. This follow-up study is the first that specifically investigates the long-term biological response until full material degradation and beyond (24 months in total). We also report on the local distribution, bony incorporation, and local clearance of Mg- and Y-ions during material degradation.

2. Material and methods

2.1. Experimental design

Surgical treatment, μCT and histological examination were performed in accordance with the preliminary study of Kraus et al. [5]. The animal experiments were performed with ethical respect for animals and were ethically approved by the Austrian Ministry of Science and Research (accreditation number BMWF-66.010/0113-II/10b/2009). Male Sprague–Dawley rats with body weights of 140–160 g and age of 5 weeks were used. The animals were housed in groups of four in clear plastic cages on standard bedding and allowed water and a standard pellet diet *ad libitum*.

Thirty-eight rats were divided into two groups: the "continuous-μCT" group ($n = 16$) and the "histological" group ($n = 22$). Each rat in these groups received two identical pins of either alloy WZ21 or alloy ZX50, which were implanted into the femoral bones.

The pins were dry-machined from extruded ZX50 and WZ21 profiles to cylindrical shapes of 8 mm length and 1.6 mm diameter. After machining they were cleaned in a cascade of pure ethanol in an ultrasonic bath and dried in warm air. Table 1 shows the nominal compositions and the mechanical characteristics of ZX50 and WZ21. A total of 76 pins were implanted.

2.2. Micro-Computed Tomography

Continuous μCT and histological evaluations were performed at months 9, 12, 15, 18 and 24 after surgery. A detailed description of the μCT evaluation and histological examination was given by Kraus et al. [5].

2.3. LA-ICP-MS

Laser Ablation Inductively Coupled Plasma Mass Spectrometry (LA-ICP-MS) measurements were applied to investigate the newly formed cortical bone area adjacent to WZ21 implants at 1, 9, 15, and 24 months after implantation. The samples were explanted, embedded in light-curing resin and cut through the central axis of the implant analogously to the histologic examinations.

The resulting sections were investigated by LA-ICP-MS, using a 266 nm Nd:YAG Laser (CETAC LSX-200, Cetac, Omaha, Nebraska, USA), which was operated at 100% energy level and 10 Hz repetition rate in lines parallel to the implant axis in defined increments. The spot diameter of the laser was 50 μm and the scan speed was set to 10 $\mu m\, s^{-1}$. The ablated material was transported via an argon carrier gas flow of 1 $L\, min^{-1}$ directly into a quadrupole ICP-MS (ELAN DRC-e, PerkinElmer, Waltham MA, USA), which was operated in standard mode. Transient signals of ^{13}C, ^{25}Mg, ^{31}P, ^{44}Ca and ^{89}Y were recorded during ablation. All signals were corrected for the gas blank, which was recorded during one minute prior to each measurement, resulting in a total of 90 data points. This gas blank was also used to calculate the limits of detection (LOD) for each individual isotope based on $LOD = \text{average} + 3\ \sigma$, with σ as the standard deviation of the measured gas blank signal intensities. Subsequently, the average of the gas blank intensities was subtracted from each individual value recorded during bone ablation, and each individual value $<LOD$ was set to zero. A moving average of 5 values was used for further evaluation, producing a spatial resolution in the scan direction of about 20 μm. To identify the mineralized bone material, a threshold value considering the Ca signal intensity and the carbon to phosphor ratio was deployed. The threshold was set to Ca intensities of <10,000 cps and C/P ratios of >0.03. These values are based on the measurement of pure hydroxyapatite standards, a hydroxyapatite matrix of fresh bones and NIST SRM 1486 (NIST, Gaithersburg MD, USA) bone reference material. The threshold was applied in order to facilitate the quantification of elements in mineralized bone structures by excluding the areas of bone marrow, embedding material and the implanted pin. The elemental mass fraction of Mg was quantified by using a NIST SRM 1486 (NIST, Gaithersburg MD, USA) as standard after normalization of the elemental signal to the ^{31}P signal. Y was quantified by using a doped HAP powder (Synthetic > 99.995%, Merck, Darmstadt, Germany), which was pressed into a pellet for further LA-ICP-MS measurements. Part of the pellet was dissolved in HNO_3/H_2O_2 (both p.a. quality, Merck) using microwave-assisted

Table 1
Nominal compositions in wt% and mechanical properties of alloys ZX50 and WZ21.

Alloy	ZX 50	WZ 21
Nominal compositions (wt%)		
Mg	Balance	Balance
Zn	5	1
Ca	0.25	0.25
Mn	0.15	0.15
Y	–	2
Biomechanical characteristics		
Yield stress	210 MPa	150 MPa
Ultimate tensile strength	295 MPa	250 MPa
Uniform elongation	18%	20%
Elongation at fracture	26%	28%

digestion and quantified by solution-based ICP-MS. ^{31}P was chosen as internal standard as P is homogeneously distributed as constituent of the mineralized bone material (hydroxyapatite). Ca was not applied as a preferred internal normalization standard because Mg can potentially substitute Ca during biodegradation of the pin material. After data reduction, the transient signals were converted and assigned to coordinates considering the laser scan speed. The resulting chemical images were produced using ArcGIS (Esri, Redlands, CA, USA). As a final step, mean values and standard deviations of the Mg and Y mass fractions were calculated separately for each line in the upper and lower cortical bone, and expressed as relative changes to the respective basal levels. In addition, the relative Ca/P ratio was calculated.

3. Results

Eight rodents died from age-related weakness and pin dislocation was observed in 5 femora. Thus fifty-five Mg pins remained for long-term analysis. The presented μCT sections, histological sections, and laser ablation images are representative examples of the respective periods of *in vivo* investigation.

3.1. Degradation performance and biological response of ZX50

The degradation behavior of ZX50 during the first 9 months was already reported by Kraus et al. [5]. After 4 months the ZX50 pins showed full degradation and further bone remodeling occurred during the follow-up observations.

In the present study, the medullary cavity showed almost full remodeling after 9 months (see Fig. 1). Neither implant debris nor corrosion products could be seen, and only small islets of bony trabecula formation were present in the medullary cavity (Fig. 2a–j). The enlarged stainings (Fig. 2b, d, f, h, j) showed predominantly adipocytes in the medullary cavity and no increased occurrence of inflammatory cells.

3.2. Degradation performance and biological response of WZ21

The degradation of the WZ21 pins was examined by *in vivo* μCT from months 9 to 24 at intervals of 3 months until month 18. Fig. 3 shows the degradation behavior of the WZ21 implant as revealed by continuous 2D μCT scans and 3D reconstructions. Intramedullary pin sections degraded within 12 months, whereas cortical implant parts remained in place for up to 18 months. Obviously, the implant in the area of the cortical bone showed a delayed degradation tendency compared to that in the medullary cavity. Residuals of the implant at the site of the bone cortex were observed up to 18 months (Fig. 3g). Full implant degradation appeared at 24 months (Fig. 3i), as confirmed by qualitative μCT and histological analysis (Fig. 4i). (Quantitative μCT analysis of pin degradation was not possible due to the fact that the magnesium alloy could not always be clearly distinguished from the surrounding bone.)

Fig. 4 illustrates the biological response on the basis of histological stainings generated on explanted bone segments at 9, 12, 15, 18, and 24 months after implantation. Bone formation appeared at the pin site during implant degradation (Fig. 4a–h), and cortical bone was detected in direct adhesion to the implant without the formation of a fibrous capsule (Fig. 4a, c, e, g). After full implant degradation at 24 months no cortical defects remained, and only tiny intramedullary islets of bony trabeculae were identified in the medullary cavity, microscopically (Fig. 4i) and via 2-D μCT scans (Fig. 3i).

Hydrogen gas bubbles were visible until 12 months after implantation (Figs. 3a, c and 4a–d), which produced little areas of cell displacement around the implant (Fig. 4e, g). The repopulation of these areas occurred mostly with adipocytes (Fig. 4e–j). Compared to the preexisting intramedullary matrix the local cell density in these regions was slightly lower, but the size of these areas shrank continuously after full pin degradation (Fig. 4i).

No pathological increase in inflammatory cells—such as leucocytes or plasma cells—in response to foreign objects was observed in histological stainings over the whole examination period (Fig. 4f, h, j).

3.3. Mg-distribution and Ca/P ratio

Fig. 5a–h illustrates the Mg mass fraction and Ca/P molar ratio in the mineralized cortical bone relative to the basal level of the respective bone. The LA-ICP-MS investigations were carried out adjacent to the pin upon degradation of the WZ21 implant. During the first months of pin degradation a significant increase in Mg was observed in the cortical bone up to approximately 2–3 mm from the pin boundary. An increase of the Mg mass fraction up to 50% from the basal level was measured (Fig. 5a, b).

The increasing dissolution of the implant generated significantly increased Mg concentrations in the cortical bone near the remaining implant parts from months 9 to 15. Increased Mg mass fractions of about one order of magnitude were observed in the lower cortical bone area of one example (month 15; Fig. 5e, f), where pin residuals were still present. In contrast, areas of fully degraded implant parts—where re-mineralization had already occurred—showed only slightly increased Mg levels (up to 20%) (Fig. 5c–f). After 24 months the Mg concentrations of undisturbed bone areas and in the area of newly formed bone at the former implant site overlap within the measurement uncertainties and show therefore no significant difference (Fig. 5g, h).

In the medullary bone area, no significant changes in the bone could be observed. Even though similar increased levels of Mg were observed close to the pin boundary, no significant Mg enrichment was detected in the newly formed bone area.

In contrast to high Mg concentrations measured in the area directly adjacent to the pin from the first months, the molar Ca/P ratio of this area did not significantly differ from the ratio of undisturbed (basal) hydroxyapatite (Fig. 5b). Between 9 and 15 months a steady decrease in the Ca/P ratio up to 20% was measured in the adjacent pin areas (Fig. 5d, f). After 24 months the Ca/P ratios showed no significant different molar ratios anymore throughout the whole cortical bone in correspondence to apatite in the cancellous bone (Fig. 5h). The cancellous bone material in the medullary area also showed no distinct variation in the Ca/P ratio throughout the whole degradation process.

3.4. Yttrium distribution

Fig. 6a–d depicts the Y mass fraction in the mineralized cortical bone directly adjacent to the pin relative to the basal level (which was about 100 ng g^{-1}). Even after just one month (Fig. 6a) the degradation of the material resulted in an enrichment of Y in the boundary region adjacent to the implant. Even though the Y content was still low compared to that observed during the subsequent degradation process, high variations in Y distribution (regions of 10-fold differences in the concentration vs. regions with basal Y levels) were already observed (reflected by the error bars in Fig. 6a). After 9 months (Fig. 6b) the Y mass fraction in the cortical bone showed a distinct increase at the pin boundary, with pronounced variations in the Y mass fraction (reflected by the large error bars). This phenomenon became even more pronounced as the degradation process advanced. The Y concentration increased locally by almost three orders of magnitude compared to the basal level in the bone after 15 months (Fig. 6c), and the variation within

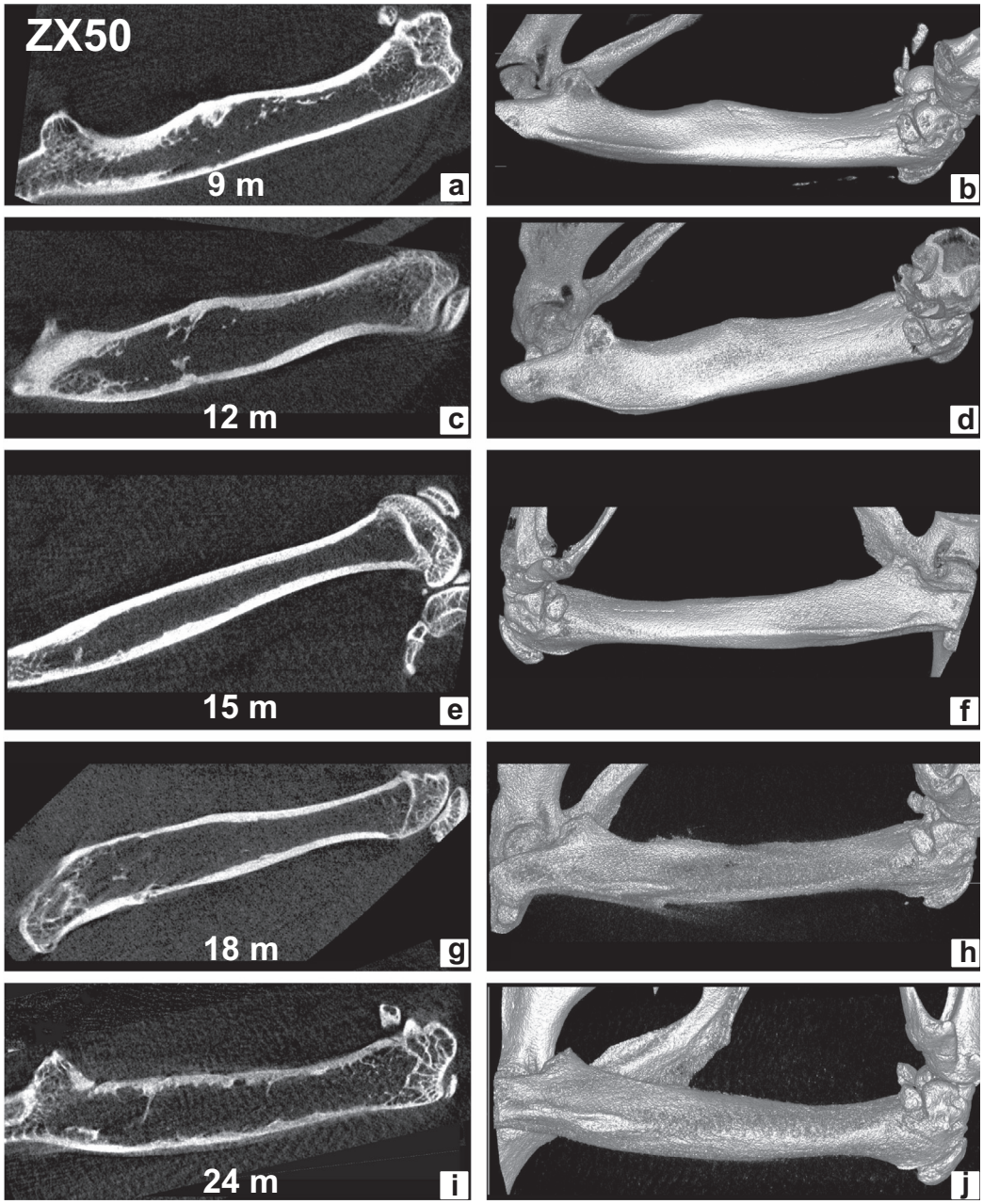

Fig. 1. 2-D μCT slices (left) and 3-D μCT reconstructions (right) illustrating the long-term bone response (⩾9 months) of the ZX50 implants. The ZX50 implant degraded completely within 4 months [5]. Intramedullar surrounding bony parts at the implant site are still detectable until month 12 (a,c), accompanying discrete remaining callus formation at the cortical site (b,d). After 15 months, the bone has healed *restitutio ad integrum* (e–j).

up to 2 mm from the pin boundary was almost two orders of magnitude. The large variations can be interpreted as migration of metallic particles. However, after 24 months (Fig. 6d), when the pin was fully degraded, the Y concentration had reached nearly basal levels within the entire cortical bone area.

4. Discussion

The objective of this study was to evaluate the long-term degradation behavior of Mg implants, and to examine the bone-implant interface and the biological response until complete degradation of the implant and beyond. Two Mg alloys were deployed: the quite rapidly degrading REE-free alloy ZX50 and the slowly degrading Y-containing alloy WZ21. After complete degradation the bones recovered completely without remaining functional disturbances, independent of the material used. Using Laser Ablation Inductively Coupled Plasma Mass Spectrometry (LA-ICP-MS)—a technique that is preferred in chemical imaging of biological tissues such as bones and teeth due to its high sensitivity, low detection limits, good accuracy and precision [32–34]—we also paid special attention to the local distribution and bony incorporation of Mg and Y ions during implant degradation. Temporary incorporation of Mg and Y into the cortical bone was detected, but also migration of Y-containing intermetallic particles. The latter one is reflected by the locally high Y values found during laser ablation.

The alloy ZX50 corroded very fast, reaching full degradation within 4 months. Despite extensive ion release and hydrogen gas formation during the first period of degradation [5], the bones recovered very well. While after 12 months slight callus formation could still be observed, the femurs healed *restitutio ad integrum*

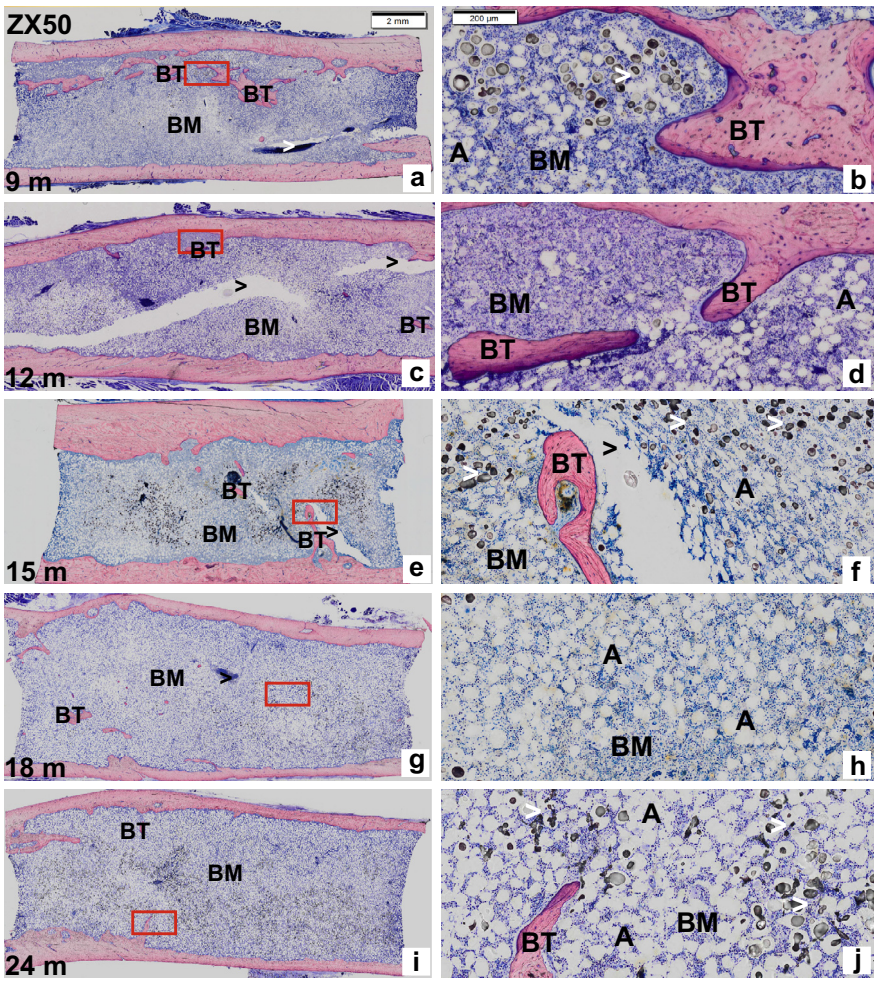

Fig. 2. Histological overview slides of ZX50 from months 9 to 24 (left-hand side) and enlarged recordings of the stainings (right-hand side, representing the respective red boxes). The cortical bones show no defects (a,c,e,g,i). In the medullary cavity, only small islets of bony trabeculae were detectable (a–j). Adipocytes predominated the medullary cavity. BT = bony trabecula, A = adipocytes, BM = bone marrow, > = preparation artifacts in the form of elongated areas and round particles.

after 15 months. Some questions concerning the ion release of ZX50 during degradation are discussed below, together with a critical view on Mg-alloy WZ21.

WZ21 degraded with significant dependence on the surrounding environment: cortical pin parts remained much longer than intramedullar implant sections. This phenomenon was first mentioned by Earl McBride in the late 1930 s, when he noticed that Mg alloy plates and intramedullary pegs corroded faster than intraosseous implants [35]. Similarly, Xu et al. reported that MgMnZn alloys degrade more rapidly in the medullary cavity than in cortical bone [36], and Gu et al. explored faster corrosion in the distal femur than in the bone marrow cavity of the diaphyseal region [37]. This may be caused by the close contact to blood vessels and the rich supply of body fluids [37,38].

Mg ion release in combination with an increase in local pH values and Ca and P depositions are indications for the activation of osteoblasts and osteocytes, generating macroscopically visible new bone formations around the implant [10,13,39–41]. In accordance with this, we observed newly formed bone around the implant in the medullar cavity and new endosteal bone formation overarching to the cortical bone. On the other hand, accelerated intramedullary degradation of Mg led to unfavorable formation of hydrogen gas due to the chemical reaction of $Mg + 2H_2O \rightarrow Mg(OH)_2 + H_2$ [42]; demonstrated in detail by Kraus et al. [5]. The water content and the local blood flow around the implant are considered the strongest determinants of local diffusion and solubility of hydrogen in surrounding tissues [30,43]. In the slowly degrading WZ21 quite small gas bubbles occurred during the degradation process in the medullary cavity, suggesting that the local hydrogen saturation of blood and tissues was exceeded at some degradation steps. Consequently, small areas of total tissue displacement in the vicinity of the degrading implant were observed in histological stainings (Fig. 4e, g, i, j). In further stages, refilling with cells occurred slowly but continuously. The long-term observations of the biological response of ZX50 and WZ21 implants revealed no long-term deficits due to cell displacement, even if a large amount of initial hydrogen gas release led to a temporary disturbance of the bone structure within the first period after pin implantation, as shown for alloy ZX50 by Kraus et al. [5]. Nevertheless, for clinical application a low hydrogen gas release is of importance, because the absorption ability of local tissues is limited and extensive gas formation may affect fracture consolidation.

The tolerance limits of Mg ion release are usually not exceeded during Mg implant degradation. Gu et al. reported that even at their fastest degradation rate Mg–Ca binary alloys ($DR \approx 3\ mg\ cm^{-2}\ d^{-1}$) could be considered for safe application, because the daily amount of Mg release would be still at milligram level and far below the daily allowance of Mg uptake ($0.7\ g\ d^{-1}$) [44–46]. For ZX50 the highest degradation rate was observed

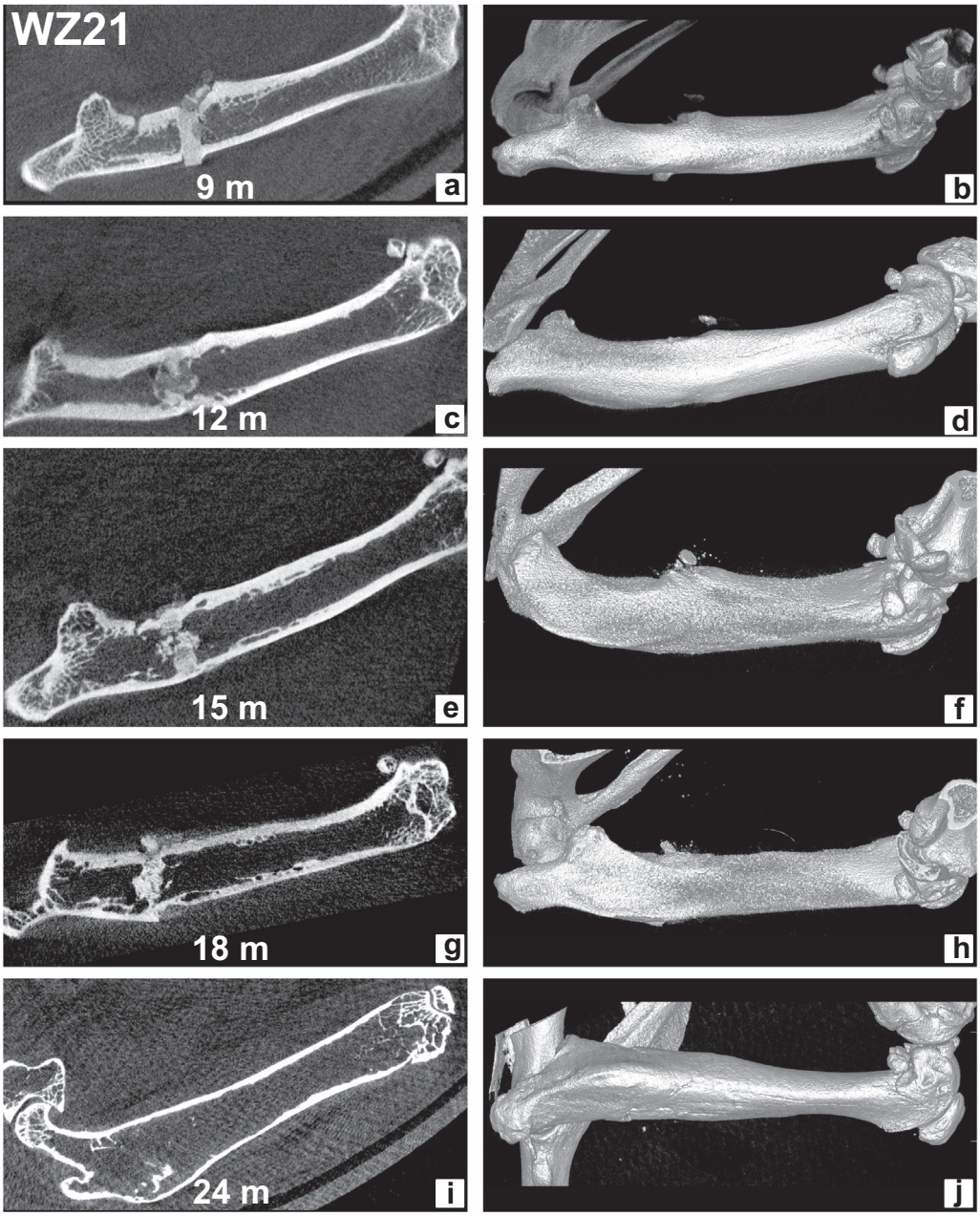

Fig. 3. 2-D μCT slices (left) and 3-D μCT reconstructions (right) illustrating the degradation process of bicortically inserted WZ21 implants and their bone response from months 9–24. After 9 months, the pin still appears in cylindrical shape (a); after 12 months severe degradation in the medullary cavity is observed (c); simultaneous to the degradation of the implant, new bone formation occurs at the pin site (c, e, g); after 24 months no pin material is detected and the bone shows full recovery (i). 3-D μCT reconstructions show callus formation at the cortical bone (b, d, f, h) and complete realignment of the cortex after 24 months (j).

between months 1 and 2 at ≈0.82 mg cm^{-2} d^{-1}, and for WZ21 between months 5 and 6 at ≈0.48 mg cm^{-2} d^{-1} [5]. Translated to a clinical setting, a daily Mg release of ≈2.6 mg d^{-1} and ≈1.5 mg d^{-1}, calculated for an intramedullary nail of 20 cm in length and 4.5 mm in diameter (which, according to the biomechanical properties of Mg-alloys, represents an effective stabilization method compared to the traditional usage of two titanium or steel nails) would remain considerably below the recommended daily uptake of a four-year-old child (130 mg d^{-1}) [47]. Homeostatic control of serum Mg concentrations by the kidneys, as well as variations in Mg serum concentrations due to Mg implant degradation, have been disproved by many studies [3,10,37,48]. Besides the kidneys, an additional homeostatic control is bone, which provides a reservoir of large concentrations of Mg to buffer acute changes in serum Mg levels [48,49].

In this study, during the first months of WZ21 degradation LA-ICP-MS measurements revealed increased Mg concentration in the mineralized matrix areas adjacent to the pin. Nevertheless, the Ca/P molar ratio in the area of >1 mm corresponded to the ratio in the basal cortical bone, indicating the same molar ratio as in undisturbed hydroxyl apatite. At later stages when pin degradation was well advanced (9 months), only slightly increased Mg levels of up to 20% compared to those in the basal area appeared in the adjacent bone matrix. This indicates that most Mg ions were already mobilized and not incorporated into the mineralized tissue. Most areas still consisted of fully mineralized hydroxyapatite, as no distinct changes were noted in the Ca/P ratio. Only in the directly adjacent pin area were noticeably increased Mg levels accompanied by a slight decrease in the Ca/P ratio measured—which may indicate the substitution of Ca by Mg at these sites. Increased Mg

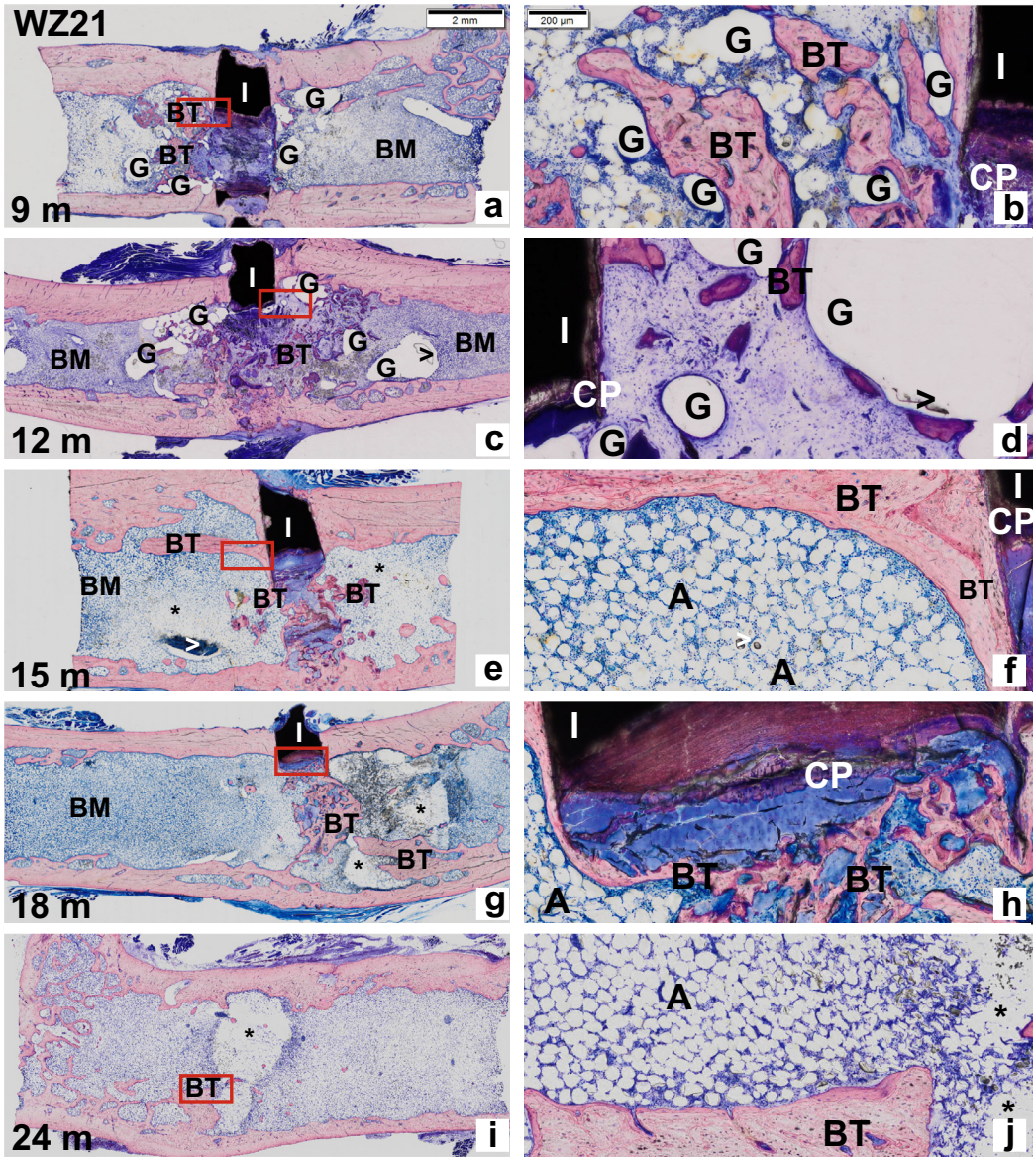

Fig. 4. Histological overview slides of WZ21 from 9 to 24 months (left-hand side) and enlarged recordings of the stainings (right-hand side, representing the respective red boxes). Remaining parts of the pin are detectable until month 18 (a–h), while after 24 months only bony trabeculae could be identified within the medullary cavity (i, j). I = implant/initial implant site, CP = corrosion products, G = gas bubble, BT = bony trabecula, A = adipocytes, BM = bone marrow, * = areas with fever cells after gas release, > = preparation artifacts in the form of elongated areas and round particles.

levels due to accumulation only seem to remain locally next to pin-degradation areas at cortical sites—which can be understood by the fact that blood flow and washout in these areas are diminished (Fig. 5e). Reduced Ca/P levels in this area also indicate a re-mineralization process where Ca was partially substituted by Mg. At this stage it is unclear whether Ca substitution by Mg has an effect on the mechanical stability of the bone matrix. However, full regeneration and restoration of the bone matrix was observed after complete pin degradation, underlined by the fact that neither Mg enrichment nor inhomogeneous Mg/Ca and Ca/P ratios were observed after 24 months.

Alloying of Y and other REEs is commonly used to improve the mechanical properties and corrosion resistance of magnesium alloys [24,50]. However, the toxicology and metabolic pathways of Y and other REEs are still unclear. It has been reported that Y^{3+} can bind to globulin and DNA [51], and uses transferrin as a binding protein in blood plasma [52]. Inhaled Y or intravenously injected YCl_3 was found to be translocated to the skeleton and taken up by phagocytes of the liver and spleen in rats [53,54]. The growth of mice was also suppressed when they received 5 ppm of Y^{3+} in their drinking water [55].

Before discussing the local distribution of Y around the degrading implant we will first consider the microstructure of WZ21, with special emphasis on the Y distribution within the microstructure. Fig. 7 shows a typical image of the microstructure, generated by transmission electron microscopy [56]. Of particular interest is the presence of relatively large ($d \approx 5$ µm) intermetallic phases (IMPs) of type $Mg_{12}YZn$ [56]. Obviously, some of the Y is not in solid solution but consumed by the IMPs. Because the alloy was extruded to rods at 380 °C and afterwards rapidly cooled to room temperature, we calculated the fraction of $Mg_{12}YZn$ and the remaining Y content in the Mg matrix at this temperature using the PANDAT algorithms with database PanMg_2013 [57]. This resulted in 5.3 mol% $Mg_{12}YZn$, with a Y content of ≈20 wt%, and

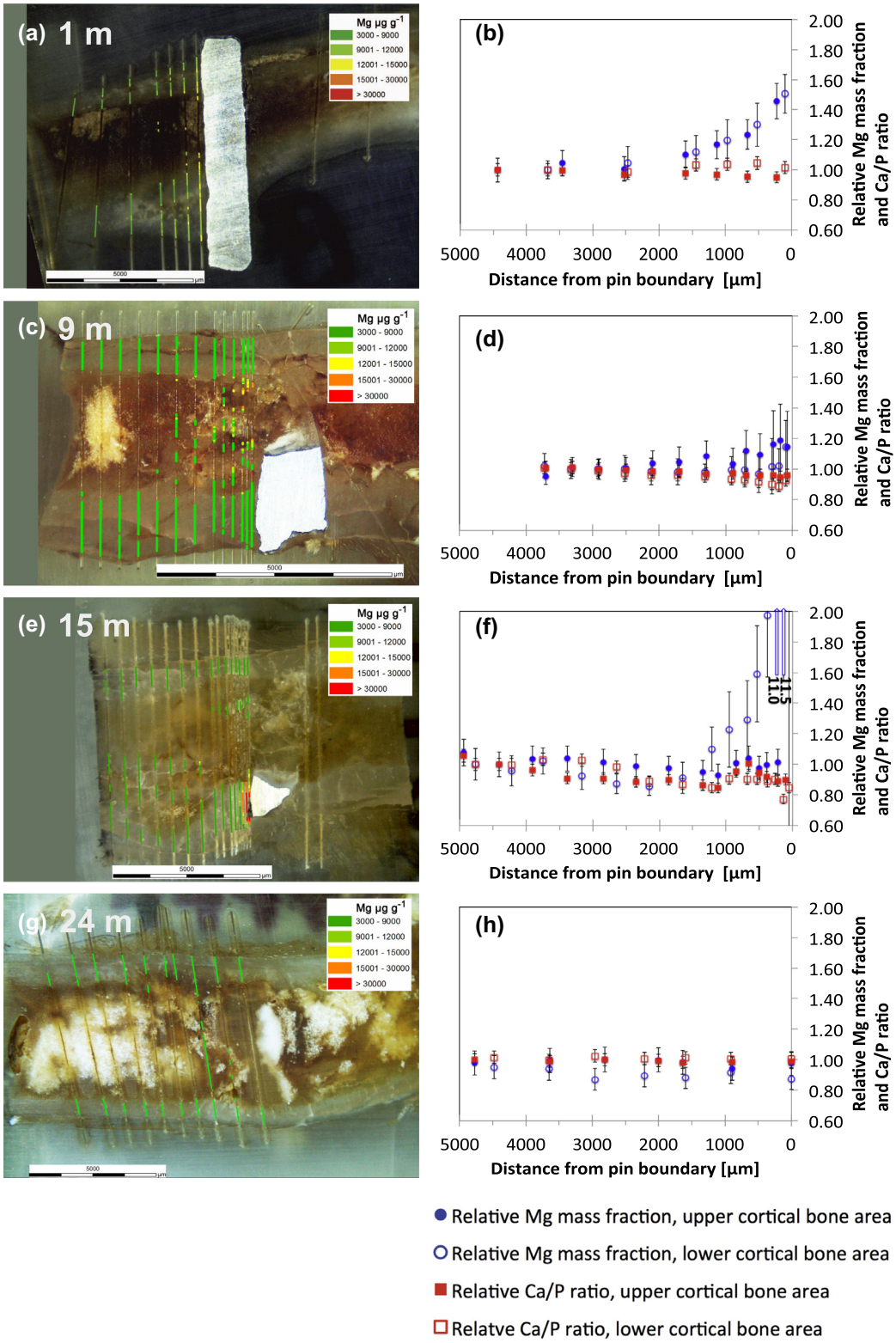

Fig. 5. LA-ICP-MS measurements after 1, 9, 15 and 24 months: The left-hand side shows the resulting chemical images: nearly all of the pin remained after 1 month (a); continual degradation of the pin after 9 and 15 months (c,e); full pin degradation at 24 months (g). The right-hand side (b,d,f,h) shows the Mg mass fraction (solid blue circles for upper cortical bone, open blue circles for lower cortical bone) and the Ca/P ratio (solid red squares for upper cortical bone, open red squares for lower cortical bone) relative to the basal level for the upper and lower cortical bone areas. Error bars represent standard deviations.

0.69 wt% Y in the matrix. Thus we can assume that only about 1/3 of the alloyed Y is in solid solution whereas the rest is incorporated into intermetallic particles.

Degradation of Mg alloys containing intermetallic particles is assumed to take place via anodic dissolution of the Mg matrix, releasing Mg ions and solute foreign atoms, in our case Y, and

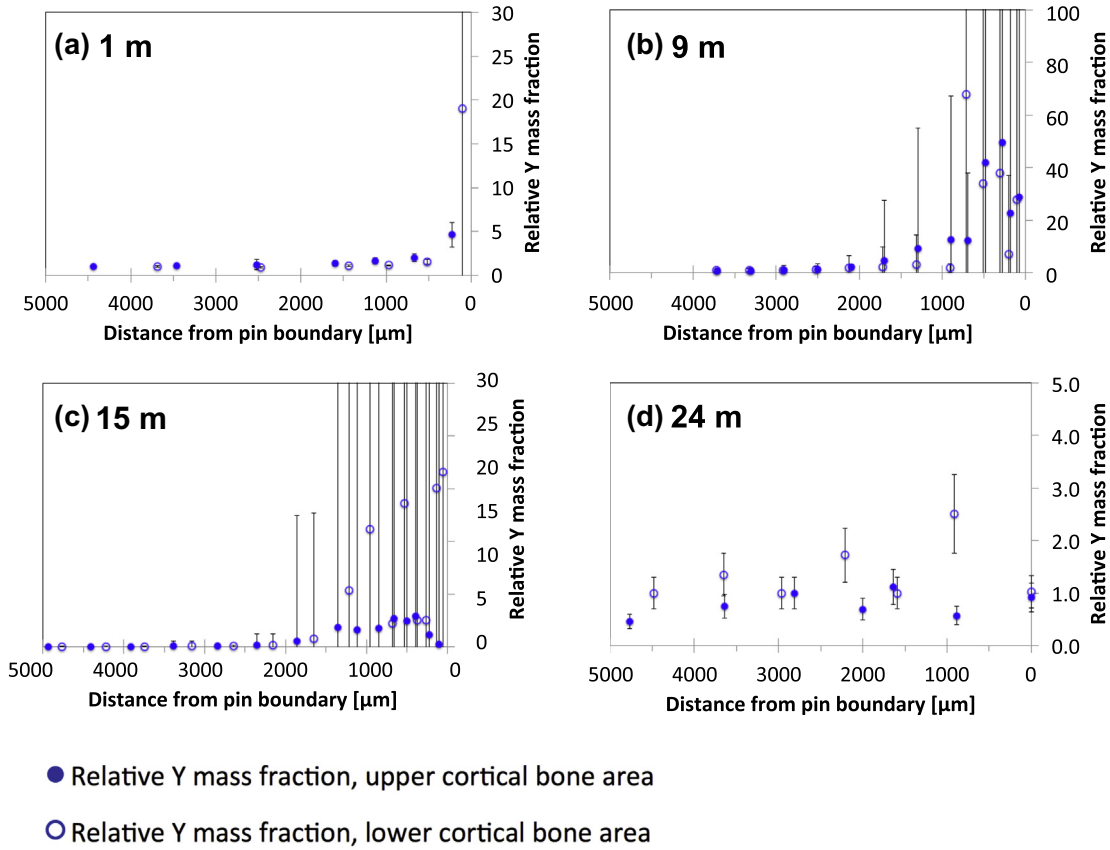

Fig. 6. LA-ICP-MS measurements after 1, 9, 15 and 24 months illustrating the Y mass fraction relative to the basal level for the upper (solid blue circles) and lower (open blue circles) cortical bone areas (a–d). Error bars represent standard deviations.

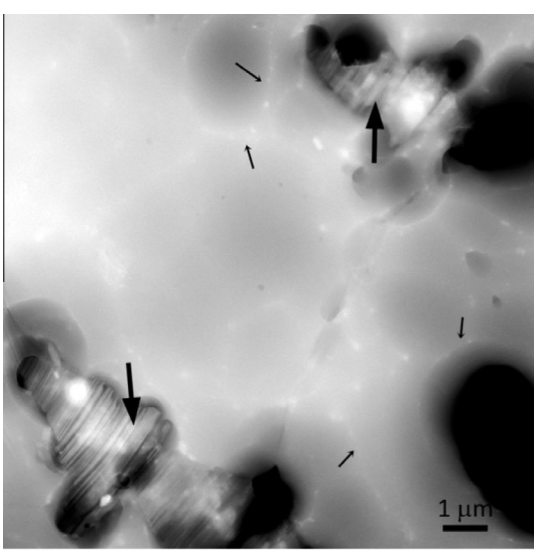

Fig. 7. TEM micrograph of as-extruded WZ21 showing particles with ordered arrays of stacking faults, typical of $Mg_{12}YZn$ (large arrows), and grain boundaries decorated with small Mg_2Ca intermetallic particles (small arrows). The black regions correspond to holes in the TEM specimen [56].

leaving behind the more noble intermetallics, in our case $Mg_{12}YZn$ [50]. The LA-ICP-MS results revealed a distinct increase in the Y content at the pin boundary even at early stages of the degradation process. With advanced degradation large amounts of Y occurred not only at the pin boundary, but also further away in cortical bone and newly formed bone inside the medullary space. As mentioned above, two Y sources must be considered: Y in solid solution and Y bound in $Mg_{12}YZn$ intermetallics. The locally very high concentrations far away from the corroding pin may indicate migration not only of released Y ions, but also of $Mg_{12}YZn$ particles. After complete pin degradation and bone remodeling, however, no Y remained locally in the bone matrix and the majority of Y seems to be mobilized and evacuated.

According to Hirano and Suzuki [58] it is not clear which cells within the bone take up most of the REEs, e.g. macrophages or erythroid cells. In any case their clearance from the bone is known to be very slow [58]. In our study we observed areas of reduced cell population at the former pin site, which may be due to former gas formation and/or the delayed evacuation of Y-containing intermetallic particles. To verify a safe excretion of Y, further studies are required to demonstrate the absence of systemic toxicity, for example via organ pathology.

5. Conclusions

The long-term effects of two different magnesium alloys and the corresponding bone response and local distribution of released ions were investigated in a growing-rat model by continuous *in vivo* µ-CT monitoring and Laser Ablation Inductively Coupled Plasma Mass Spectrometry (LA-ICP-MS). A rapidly degrading magnesium alloy (ZX50) and a slowly degrading alloy (WZ21) were tested. The following statements can be made:

- Bone recovers *restitutio ad integrum* after complete degradation of the magnesium implant, in both the more slowly degrading Y-containing alloy WZ21 and the rapidly degrading alloy ZX50, where massive gas formation is temporarily observed.

- Degradation of the Mg alloy generates a significant increase in Mg concentration in the cortical bone near the remaining implant parts. After complete degradation, however, no difference in Mg content between undisturbed bone areas and newly formed bone at the former implant site is seen.
- During degradation of alloy WZ21 large amounts of Y were measured not only at the pin boundary, but also farer away in cortical bone and in newly formed bone inside the medullary space. The locally high Y concentrations suggest migration of both Y ions and Y-containing intermetallic particles. After full degradation of the implant Y-enrichment in bone tissues disappeared almost completely.
- It is recommended to verify a safe excretion of Y, for example by organ pathology, to demonstrate the absence of systemic toxicity for rare-earth-element containing biodegradable implants.

Acknowledgements

The authors appreciate support from the Laura Bassi Center of Expertise BRIC (Bioresorbable Implants for Children; FFG, Austria) and from the degIMMAT project (LS11-009) funded by the NÖ Forschungs-und Bildungsges. m. b. H. (NFB, Austria). The authors would also like to thank Mag. Stefan Tangl (Department of Oral Surgery, Medical University of Vienna, Austria) for the histological workup of the specimens.

References

[1] F.I. Wolf, A. Cittadini, Chemistry and biochemistry of magnesium, Mol. Aspects Med. 24 (1–3) (2003) 3–9.
[2] R.D. Grubbs, M.E. Maguire, Magnesium as a regulatory cation: criteria and evaluation, Magnesium 6 (3) (1987) 113–127.
[3] N.E. Saris, E. Mervaala, H. Karppanen, J.A. Khawaja, A. Lewenstam, Magnesium. An update on physiological, clinical and analytical aspects, Clin. Chim. Acta 294 (1–2) (2000) 1–26.
[4] G.A. Quamme, Renal magnesium handling: new insights in understanding old problems, Kidney Int. 52 (5) (1997) 1180–1195.
[5] T. Kraus, S.F. Fischerauer, A.C. Hänzi, P.J. Uggowitzer, J.F. Löffler, A.M. Weinberg, Magnesium alloys for temporary implants in osteosynthesis: in vivo studies of their degradation and interaction with bone, Acta Biomater. 8 (3) (2012) 1230–1238.
[6] M.P. Staiger, A.M. Pietak, J. Huadmai, G. Dias, Magnesium and its alloys as orthopedic biomaterials: a review, Biomaterials 27 (9) (2006) 1728–1734.
[7] H. Zreiqat, C.R. Howlett, A. Zannettino, P. Evans, G. Schulze-Tanzil, C. Knabe, M. Shakibaei, Mechanisms of magnesium-stimulated adhesion of osteoblastic cells to commonly used orthopaedic implants, J. Biomed. Mater. Res. 62 (2) (2002) 175–184.
[8] Y. Yamasaki, Y. Yoshida, M. Okazaki, A. Shimazu, T. Uchida, T. Kubo, Y. Akagawa, Y. Hamada, J. Takahashi, N. Matsuura, Synthesis of functionally graded MgCO3 apatite accelerating osteoblast adhesion, J. Biomed. Mater. Res. 62 (1) (2002) 99–105.
[9] Y. Yamasaki, Y. Yoshida, M. Okazaki, A. Shimazu, T. Kubo, Y. Akagawa, T. Uchida, Action of FGMgCO3Ap-collagen composite in promoting bone formation, Biomaterials 24 (27) (2003) 4913–4920.
[10] Z. Li, X. Gu, S. Lou, Y. Zheng, The development of binary Mg-Ca alloys for use as biodegradable materials within bone, Biomaterials 29 (10) (2008) 1329–1344.
[11] P.A. Revell, X.S. Zhang, P. Evans, C.R. Howlett, The effect of magnesium ions on bone bonding to hydroxyapatite, Key Eng. Mater. 254–256 (2004) 447–450.
[12] R.A. Lindtner, C. Castellani, S. Tangl, G. Zanoni, P. Hausbrandt, E.K. Tschegg, S.E. Stanzl-Tschegg, A.M. Weinberg, Comparative biomechanical and radiological characterization of osseointegration of a biodegradable magnesium alloy pin and a copolymeric control for osteosynthesis, J. Mech. Behav. Biomed. Mater. 28 (2013) 232–243.
[13] F. Witte, V. Kaese, H. Haferkamp, E. Switzer, A. Meyer-Lindenberg, C.J. Wirth, H. Windhagen, In vivo corrosion of four magnesium alloys and the associated bone response, Biomaterials 26 (17) (2005) 3557–3563.
[14] S.F. Fischerauer, T. Kraus, X. Wu, S. Tangl, E. Sorantin, A.C. Hänzi, J.F. Löffler, P.J. Uggowitzer, A.M. Weinberg, In vivo degradation performance of micro-arc-oxidized magnesium implants: a micro-CT study in rats, Acta Biomater. 9 (2) (2013) 5411–5420.
[15] X. Gu, Y. Zheng, Y. Cheng, S. Zhong, T. Xi, In vitro corrosion and biocompatibility of binary magnesium alloys, Biomaterials 30 (4) (2009) 484–498.
[16] G. Song, Control of biodegradation of biocompatable magnesium alloys, Corros. Sci. 49 (4) (2007) 1696–1701.
[17] F. Witte, J. Fischer, J. Nellesen, H.A. Crostack, V. Kaese, A. Pisch, F. Beckmann, H. Windhagen, In vitro and in vivo corrosion measurements of magnesium alloys, Biomaterials 27 (7) (2006) 1013–1018.
[18] C.E. Wen, M. Mabuchi, Y. Yamada, K. Shimojima, Y. Chino, T. Asahina, Processing of biocompatible porous Ti and Mg, Scripta Mater. 45 (10) (2001) 1147–1153.
[19] E. Zhang, L. Xu, G. Yu, F. Pan, K. Yang, In vivo evaluation of biodegradable magnesium alloy bone implant in the first 6 months implantation, J. Biomed. Mater. Res. A 90 (3) (2009) 882–893.
[20] M.B. Kannan, R.K. Raman, In vitro degradation and mechanical integrity of calcium-containing magnesium alloys in modified-simulated body fluid, Biomaterials 29 (15) (2008) 2306–2314.
[21] W.D. Mueller, M.F. de Mele, M.L. Nascimento, M. Zeddies, Degradation of magnesium and its alloys: dependence on the composition of the synthetic biological media, J. Biomed. Mater. Res. A 90 (2) (2009) 487–495.
[22] B. Zberg, P.J. Uggowitzer, J.F. Löffler, MgZnCa glasses without clinically observable hydrogen evolution for biodegradable implants, Nat. Mater. 8 (11) (2009) 887–891.
[23] C. Castellani, R.A. Lindtner, P. Hausbrandt, E. Tschegg, S.E. Stanzl-Tschegg, G. Zanoni, S. Beck, A.M. Weinberg, Bone-implant interface strength and osseointegration: Biodegradable magnesium alloy versus standard titanium control, Acta Biomater. 7 (1) (2011) 432–440.
[24] N. Hort, Y. Huang, D. Fechner, M. Stormer, C. Blawert, F. Witte, C. Vogt, H. Drucker, R. Willumeit, K.U. Kainer, F. Feyerabend, Magnesium alloys as implant materials–principles of property design for Mg-RE alloys, Acta Biomater. 6 (5) (2010) 1714–1725.
[25] F. Rosalbino, S. De Negri, A. Saccone, E. Angelini, S. Delfino, Bio-corrosion characterization of Mg-Zn-X (X = Ca, Mn, Si) alloys for biomedical applications, Journal of materials science, Mater. Med. 21 (4) (2010) 1091–1098.
[26] D. Dziuba, A. Meyer-Lindenberg, J.M. Seitz, H. Waizy, N. Angrisani, J. Reifenrath, Long-term in vivo degradation behaviour and biocompatibility of the magnesium alloy ZEK100 for use as a biodegradable bone implant, Acta Biomater. 9 (10) (2013) 8548–8560.
[27] M. Thomann, C. Krause, N. Angrisani, D. Bormann, T. Hassel, H. Windhagen, A. Meyer-Lindenberg, Influence of a magnesium-fluoride coating of magnesium-based implants (MgCa0.8) on degradation in a rabbit model, J. Biomed. Mater. Res. A 93 (4) (2010) 1609–1619.
[28] H. Waizy, J. Diekmann, A. Weizbauer, J. Reifenrath, I. Bartsch, V. Neubert, R. Schavan, H. Windhagen, In vivo study of a biodegradable orthopedic screw (MgYREZr-alloy) in a rabbit model for up to 12 months, J. Biomater. Appl. 28 (5) (2014) 667–675.
[29] Q. Peng, Y. Huang, L. Zhou, N. Hort, K.U. Kainer, Preparation and properties of high purity Mg-Y biomaterials, Biomaterials 31 (3) (2010) 398–403.
[30] F. Witte, N. Hort, C. Vogt, S. Cohen, K.U. Kainer, R. Willumeit, F. Feyerabend, Degradable biomaterials based on magnesium corrosion, Curr. Opin. Solid State Mater. Sci. 12 (5–6) (2008) 63–72.
[31] C. Rössig, N. Angrisani, P. Helmecke, S. Besdo, J.M. Seitz, B. Welke, N. Fedchenko, H. Kock, J. Reifenrath, In vivo evaluation of a magnesium-based degradable intramedullary nailing system in a sheep model, Acta Biomater. 25 (2015) 369–383.
[32] S.F. Durrant, N.I. Ward, Recent biological and environmental applications of laser ablation inductively coupled plasma mass spectrometry (LA-ICP-MS), J. Anal. At. Spectrom. 20 (9) (2005) 821–829.
[33] J.S. Becker, H. Sela, J. Dobrowolska, M. Zoriy, J.S. Becker, Recent applications on isotope ratio measurements by ICP-MS and LA-ICP-MS on biological samples and single particles, Int. J. Mass Spectrom. 270 (1–2) (2008) 1–7.
[34] W. Castro, J. Hoogewerff, C. Latkoczy, J.R. Almirall, Application of laser ablation (LA-ICP-SF-MS) for the elemental analysis of bone and teeth samples for discrimination purposes, Forensic Sci. Int. 195 (1–3) (2010) 17–27.
[35] E.D. McBridge, Magnesium screw and nail transfixion in fractures, South. Med. J. 31 (5) (1938) 508–515.
[36] L. Xu, G. Yu, E. Zhang, F. Pan, K. Yang, In vivo corrosion behavior of Mg-Mn-Zn alloy for bone implant application, J. Biomed. Mater. Res. A 83 (3) (2007) 703–711.
[37] X.N. Gu, X.H. Xie, N. Li, Y.F. Zheng, L. Qin, In vitro and in vivo studies on a Mg-Sr binary alloy system developed as a new kind of biodegradable metal, Acta Biomater. 8 (6) (2012) 2360–2374.
[38] N. Erdmann, N. Angrisani, J. Reifenrath, A. Lucas, F. Thorey, D. Bormann, A. Meyer-Lindenberg, Biomechanical testing and degradation analysis of MgCa0.8 alloy screws: a comparative in vivo study in rabbits, Acta Biomater. 7 (3) (2011) 1421–1428.
[39] T. Kokubo, Formation of biologically active bone-like apatite on metals and polymers by a biomimetic process, Thermochim. Acta 280–281 (1996) 479–490.
[40] N. von der Hoh, A. Krause, C. Hackenbroich, D. Bormann, A. Lucas, A. Meyer-Lindenberg, Influence of different surface machining treatments of resorbable implants made from different magnesium-calcium alloys on their degradation–a pilot study in rabbit models, Dtsch. Tierarztl. Wochenschr. 113 (12) (2006) 439–446.
[41] M. Thomann, C. Krause, D. Bormann, N. von der Höh, H. Windhagen, A. Meyer-Lindenberg, Comparison of the resorbable magnesium. alloys LAE442 und MgCa0.8 concerning their mechanical properties, their progress of degradation and the bone-implant-contact after 12 months implantation duration in a rabbit model, Materialwiss. Werkstofftech. 40 (1–2) (2009) 82–87.
[42] M. Pourbaix, Atlas of Electrochemical Eqilibria in Aqueous Solutions, National Association of Corrosion Engineers, Housten, Texas, 1974.

[43] F. Witte, J. Fischer, J. Nellesen, C. Vogt, J. Vogt, T. Donath, F. Beckmann, In vivo corrosion and corrosion protection of magnesium alloy LAE442, Acta Biomater. 6 (5) (2010) 1792–1799.
[44] X.-N. Gu, Y.-F. Zheng, A review on magnesium alloys as biodegradable materials, Front. Mater. Sci. Chin. 4 (2) (2010) 111–115.
[45] M. Kujawa, Metal Ions in Biological Systems. Circulation of metals in the environment. Herausgegeben von H. Sigel. 397 Seiten, zahlr. Abb. und Tab. Marcel Dekker Inc, New York und Basel 1984. Preis: 95.50 $, Food/Nahrung 30 (1) (1986). 107-107.
[46] H.G. Seiler, Handbook on Toxicity of Inorganic Compounds, Marcel Dekker Inc., New York, 1988.
[47] I.R.D. Intakes, Nutrient Reference Values for Australia and New Zealand, (2005) 2005.
[48] J. Vormann, Magnesium: nutrition and metabolism, Mol. Aspects Med. 24 (1–3) (2003) 27–37.
[49] R.M. Touyz, Magnesium in clinical medicine, Front. Biosci. 9 (2004) 1278–1293.
[50] J. Zhang, J. Xu, W. Cheng, C. Chen, J. Kang, Corrosion behavior of Mg–Zn–Y alloy with long-period stacking ordered structures, J. Mater. Sci. Technol. 28 (12) (2012) 1157–1162.
[51] B. Rosoff, H. Spencer, Binding of rare earths to serum proteins and DNA, Clin. Chim. Acta 93 (3) (1979) 311–319.
[52] A.W. Ford-Hutchinson, D.J. Perkins, 46 Scandium metabolism; binding to metalloproteins in vivo and in vitro, Radiat. Res. 51 (2) (1972) 244–248.
[53] S. Hirano, N. Kodama, K. Shibata, K.T. Suzuki, Metabolism and toxicity of intravenously injected yttrium chloride in rats, Toxicol. Appl. Pharmacol. 121 (2) (1993) 224–232.
[54] W.J. Wenzel, R.G. Thomas, R.O. McClellan, Effect of stable yttrium concentration on the distribution and excretion of inhaled radioyttrium in the rat, Am. Ind. Hyg. Assoc. J. 30 (6) (1969) 630–634.
[55] H.A. Schroeder, M. Mitchener, Scandium, chromium(VI), gallium, yttrium, rhodium, palladium, indium in mice: effects on growth and life span, J. Nutr. 101 (10) (1971) 1431–1437.
[56] A.C. Hänzi, A.S. Sologubenko, P.J. Uggowitzer, Design strategy for microalloyed ultra-ductile magnesium alloys for medical applications, Mater. Sci. Forum 618–619 (2009) 75–82.
[57] C.L. Pandat, Software package for calculating phase diagrams and thermodynamic properties of multi-component alloys, <http://www.computhermcom/>, 2013, Madison, WI 53719 USA.
[58] S. Hirano, K.T. Suzuki, Exposure, metabolism, and toxicity of rare earths and related compounds, Environ. Health Perspect. 104 (Suppl. 1) (1996) 85–95.